Received: 13 January 2020 | Revised: 26 June 2020 | Accepted: 29 June 2020

DOI: 10.1096/fj.202000097RR

RESEARCH ARTICLE

THE FASEB JOURNAL

Domain zipping and unzipping modulates TRPM4's properties in human cardiac conduction disease

Wenying Xian[1] | **Hongmei Wang**[2] | **Alessandra Moretti**[3,4] | **Karl-Ludwig Laugwitz**[3,4] | **Veit Flockerzi**[2] | **Peter Lipp**[1]

[1]Molecular Cell Biology, Centre for Molecular Signaling (PZMS), Medical Faculty, Saarland University, Homburg, Germany

[2]Experimental and Clinical Pharmacology and Toxicology, Centre for Molecular Signaling (PZMS), Medical Faculty, Saarland University, Homburg, Germany

[3]First Medical Department (Cardiology), Klinikum rechts der Isar, Technische Universität München, München, Germany

[4]DZHK (German Centre for Cardiovascular Research) - partner site Munich Heart Alliance, Munich, Germany

Correspondence
Peter Lipp, Molecular Cell Biology, Centre for Molecular Signaling (PZMS), Medical Faculty, Saarland University, 66421 Homburg, Germany.
Email: peter.lipp@uks.eu

Present address
Hongmei Wang, Department of Pharmacology, School of Medicine, Southeast University, Nanjing, China

Funding information
Deutsche Forschungsgemeinschaft (DFG), Grant/Award Number: SFB TRR 152; Alexander von Humboldt-Stiftung (Humboldt Foundation)

Abstract

The transient receptor potential melastatin 4 (TRPM4) is a Ca^{2+}-activated nonselective cation channel linked to human cardiac diseases. The human mutation K914R within TRPM4's S4-S5 linker was identified in patients with atrioventricular block. During UV-flash-mediated Ca^{2+} transients, $TRPM4^{K914R}$ generated a threefold augmented membrane current concomitant with 2 to 3-fold slowed down activation and deactivation kinetics resulting in excessive membrane currents during human cardiac action potentials. Mutagenesis of K914 paired with molecular modeling suggested the importance of the nanoscopic interface between the S4-S5 linker, the MHR4-, and TRP-domain as a major determinant for TRPM4's behavior. Rational mutagenesis of an interacting amino acid (R1062Q) in the TRP domain was able to offset K914R`s gain-of-function by zipping and unzipping of this nanoscopic interface. In conclusion, repulsion and attraction between the amino acids at positions 914 and 1062 alters the flexibility of the nanoscopic interface suggesting a zipping and unzipping mechanism that modulates TRPM4's functions. Pharmacological modulation of this intramolecular mechanism might represent a novel therapeutic strategy for the management of TRPM4-mediated cardiac diseases.

KEYWORDS

cardiac conduction disease, calcium, S4-S5 linker, TRP domain, TRPM4

Abbreviations: AV-blocks, atrioventricular block; FBS, fetal bovine serum; HEK293, human embryonic kidney 293; hiPSC-CMs, human-induced pluripotent stem cell-derived cardiac myocytes; K914E, mutation from lysine to glutamate at site 914; K914G, mutation from lysine to glycine at site 914; K914R, mutation from lysine to arginine at site 914; MHR, transient receptor potential melastatin subfamily homology region; NP-EGTA, *o*-Nitrophenyl EGTA; R1062Q, mutation from arginine to glutamine at site 1062; RBBB, right bundle branch block; S4, transmembrane domain 4; S5, transmembrane domain 5; TagRFPT, red fluorescent protein derived from TagRFP; TRP, transient receptor potential; TRPM4, transient receptor potential melastatin subfamily member 4; wt, wild-type.

Wenying Xian and Hongmei Wang shared first authorship.

1 | INTRODUCTION

The transient receptor potential melastatin 4 (TRPM4) channel is a Ca^{2+}-activated nonselective cation channel with a widespread expression pattern.[1] In the heart, expression of TRPM4 is prominent in the Purkinje fibers and nodal tissues.[2,3] Genetic variants in the *TRPM4* gene have been linked to various cardiac diseases including cardiac conduction defects, Brugada syndrome, and long QT syndrome.[2-5] Both, gain- and loss-of-function were reported for these TRPM4 variants.[3] In a gain-of-function variant E7K, linked to progressive familial heart block type 1, the $TRPM4^{E7K}$ protein was reported to accumulate in the plasma membrane as a result of aberrant SUMOylation of the protein.[2] A recent study suggested an altered degradation rate of the proteins as a novel mechanism for cardiac conduction diseases.[6] As shown recently, gain-of-function mutations in the S6 segment of TRPM4 channel associated with human skin diseases depicted an increased sensitivity to intracellular Ca^{2+}.[7] Our previous study revealed an isolated reduction in the Ca^{2+}-dependent deactivation of the human mutation $TRPM4^{A432T}$ as a novel etiology in the pathogenesis of cardiac arrhythmia such as cardiac conduction block.[8]

Recent reports on TRPM4's structure revealed an inverted crown-like architecture of the functional tetrameric channel protein, containing six transmembrane, the N- and C-cytosolic domains.[9,10] The most prominent feature of TRPM4 is its long N-terminal domain including four TRPM Homology Regions (MHR1-4), which are envisaged to interact with the TRP and the C-terminal domain.[11,12] Another feature of the TRPM4 protein is that its TRP domain is not continuous but fragmented into two helices. The longer one, referred as the TRP helix, follows the transmembrane helix S6 and runs parallel to the cytosolic face of the plasma membrane. The shorter one, referred to as the TRP re-entrant connects to the C-terminal domain.[10,11] The first four transmembrane domains (S1-S4) are followed by the pore-forming domains (S5-S6). The S4-S5 linker, connecting the S1-S4 helices and S5-S6 pore-forming domain, is best known for its putative contribution to channel's gating. In voltage-gated ion channels, channel opening is often coupled to the movement of S1-S4 voltage sensors through the S4-S5 linker helix, which leads to splay of the lower S6 helix and opens the activation gate.[13] In TRPV1, the S4-S5 linker and S6 interact through the hydrogen bonding between two residues, D576 in the S4-S5 linker and M684 in S6, to open TRPV1's lower gate.[14] In TRPV4, S4-S5 linker is reported to play a role in both opening[15] and stabilizing channel's closed state.[16]

Interestingly, TRP's S4-S5 linker became a hot spot for human mutations causing different channelopathies. Two missense mutations (G573S and W692G) of TRPV3 were identified in patients with Olmsted syndrome.[17] A gain-of-function mutation of TRPA1's S4-S5 linker was reported in the familial episodic pain syndrome.[18,19] At least eight of these known human TRPV4 mutants (Y591C, F592L, R594H, R594S, L596P, G600W, Y602C, I604M) locate within the S4-S5 linker, have been linked to various skeletal dysplasia and neuropathies.[20] Stallmeyer and co-workers identified a mutation K914R in the S4-S5 linker of the TRPM4 channel in two patients from the same family.[4] The son suffered from severe, congenital atrioventricular block (AVB) 3° and required implantation of a cardiac pacemaker for more than 30 years, while his father carrying the same mutation presented a less severe phenotype with a normal atrioventricular conductance and an asymptomatic right bundle branch block (RBBB).[4] However, a functional characterization of $TRPM4^{K914R}$ and the underlying etiology for the cardiac conduction block are still lacking.

In the present study, we employed a combination of electrophysiology, intracellular Ca^{2+} recordings, and rapid manipulations of Ca^{2+} by UV-flash photolysis of caged Ca^{2+} compounds[8] to gain deeper insights into the possible molecular mechanisms of a human TRPM4 mutation (K914R) mediating cardiac conduction diseases. Our results strongly suggest an etiology in TRPM4-related cardiac conduction diseases with aberrant intramolecular interfaces within the mutated TRPM4 channel resulting in zipping and unzipping of these nanodomains. We identified the S4-S5 linker—TRP domain—MHR4 interface to substantially modulate TRPM4's Ca^{2+}-dependent functional properties. Altogether, the human K914R mutation appears to be a gain-of-function mutation mediated by intramolecular weakening of this important interface.

2 | MATERIALS AND METHODS

2.1 | Cell culture and expression

Human embryonic kidney (HEK293) cells were cultured in Dulbecco's modified Eagle's culture medium supplemented with 10% (v/v) FBS, and a cocktail of 100 U/mL penicillin and 100 µg/mL streptomycin. Cells were maintained at 37°C in a humidity-controlled incubator with 5% CO_2. Prior to the experiments cells were seeded on 20 mm diameter glass coverslips in 12-well plates for electrophysiological recording or 6-well plates for western blots. 24 hours after seeding, cells were transiently transfected with 1 µg/well given plasmid by NanoJuice (Novagen, USA) following the manufacture´s instruction. After incubation for another 48-72 hours, successful transfection can be verified by the expression of TagRFPT.

2.2 | TRPM4 mutagenesis

The complete human wild-type TRPM4 cDNA was kindly provided by Dr Ulrich Wissenbach and Prof. Flockerzi

(GenBank: AF497623.1) and then, fused with a fluorescence protein TagRFPT at the C-terminus into a pCR259 vector. Mutations were obtained by a two-step PCR protocol as previously described,[21] and the mutated clones were re-sequenced before further experimental use.

2.3 | Electrophysiology

Electrophysiological recordings were performed in the whole-cell patch clamp configuration with an EPC-10 amplifier (HEKA Electronic, Germany). Patch pipettes had a resistance of 3-5 MΩ with intracellular solution contained (in mmol/L): 140 CsCl, 1 $MgCl_2$, 10 HEPES, 1 NP-EGTA, 0.5 $CaCl_2$, and 0.15 Fluo-4FF. The pH was adjusted to 7.2 with CsOH and the free Ca^{2+} concentration was determined in independent experiments by Fura-2 in vitro. Extracellular solution contained (in mmol/L): 140 NaCl, 1 $MgCl_2$, 1.8 $CaCl_2$, 10 HEPES, and 10 Glucose, pH 7.35 was adjusted with NaOH. The holding potential was set to −60 mV, the TRPM4 currents were recorded at +80 mV.

2.4 | UV-flash assay

The UV-flash assay was described in details recently.[8] In brief, a UV-flash lamp (RAPP OptoElectronic GmbH, Germany) was coupled to the inverted microscope (TE2000-U, Nikon, Japan). Brief high-intensity flashes were used to uncage Ca^{2+} from the Ca^{2+}-caged compound NP-EGTA (cat. N6802, Thermo Fisher). Excitation of the Fluo-4FF was performed centered around 480 nm (±5 nm) with a monochromator (PolyChrome V, TILL, Photonics, Germany) and the emission was collected by photodiode-based epifluorescence hardware (TILL, Photonics, Germany) via a 515 nm long-pass filter. The Ca^{2+} concentration was calculated as described previously.[8]

2.5 | Measurement and calculation of the free Ca^{2+} concentration

The procedure to construct current versus Ca^{2+} concentration relationship and the determination of the activation and deactivation was reported recently.[8]

The pipette solution without NP-EGTA and Ca^{2+} was aliquots into 100 μL with 5 mM EGTA. Then different amount of Ca^{2+} was added to the solution for the final concentrations (mM): 0.1, 0.3, 0.5, and 0.7. Then these solutions were measured separately by Fura-2 and Fluo-4, from which we could know the Fluo-4 fluorescence intensity of these solutions as well the corresponding free Ca^{2+} concentrations. Based on these results two stand curves as shown in following Figure S3. Then the fluorescence intensities of TRPM4 pipette solution with NP-EGTA (1 mM) and Ca^{2+} (0.5 mM) concentrations were measured by Fluo-4 (Figure S3A horizontal dashed line). According to the Fluo-4 fluorescence intensity curve, the corresponding Ca^{2+} was 0.31 mM (see Figure S3A vertical dashed line), which was also depicted in the Figure S3B (vertical dashed line), the corresponding free Ca^{2+} concentration was calculated according to the Fura-2 standard curve (see Figure S3B horizontal dashed line), that was about 100 nM.

In experiments, free Ca^{2+} concentration was calculated as described in our previous publication.[8] $[Ca^{2+}] = KR[(K/[Ca^{2+}]_0 + 1)-R]$. R is the fluorescence ratio and K is the dissociation constant for Fluo-4FF. $[Ca^{2+}]_0$ is the Ca^{2+} concentration of the pipette solution that was determined in independent experiments in small aliquots in vitro as described as above.

2.6 | Action potential playback

The human-induced pluripotent stem cell-derived cardiac myocytes (hiPS-CMs) were generated and cultured as described earlier.[22] Spontaneous action potentials were recorded from these cells with Tyrode solution containing (mM): 137 NaCl, 5.4 KCl, 10 HEPES, 10 Glucose, 1 $MgCl_2$, 1.8 $CaCl_2$, pH was set to 7.4 with NaOH and the internal solution contains (mM): 135 KCl, 10 NaCl, 2 $MgCl_2$, 1 EGTA, 10 HEPES, 3 MgATP, pH was adjusted to 7.2 with KOH. Typical ventricular-like action potential waveforms were selected as the command voltage template in voltage-clamp, while triggering the UV-flashes to induce Ca^{2+} release and recording the membrane currents as well as the intracellular Ca^{2+} concentration by patch clamp simultaneously.

2.7 | Surface biotinylation and Western blot

Cells were incubated with Sulfo-NHS-LC Biotin (1 mg/mL, gently shaking for 30 minutes at 4°C, cat. 21335, Thermo Fisher) to label all the surface proteins as described by the manufacture's instruction. To precipitate biotinylated proteins, supernatant containing proteins was incubated with Dynabeads MyOne Streptavidin C1 (cat. 65001, Thermo Fisher) for 30 minutes at 4°C following the protocol suggested by manufacture. Proteins were separated by NuPAGE 3%-8% Tris-Acetate Gels (EA03755BOX, Thermo Fisher) and detected with anti-tagRFPT (cat. #AB234, Evrogen), anti-Na/K+ATPase α-1N-15 (cat. #sc-16041, Santa Cruz Biotechnology) and anti-actin (cat. #sc-8432, Santa Cruz Biotechnology) antibodies.

2.8 | Confocal imaging

A TSC SP5 ll(Leica Microsystems, Wetzlar, Germany) confocal microscope based on an inverted microscope with a

high-speed resonating X-scanner and spectral emission detection was used for acquisition of confocal images. Excitation of TagRFPT was achieved with the 561 nm line of a solid state laser and images (1024 × 1024 pixels) were acquired for emission wavelengths above 565 nm with a standard PMT. The Leica Application Suite software (ver. 2.4) was used to control the confocal system.

2.9 | Model generation

Molecular dynamic simulations are performed using Materials Studio 6.0 software (Accelrys Inc, USA). The Forcite module was used to simulate the possible conformations and optimize the simulation under Compass field. Energy minimization was carried out using the steepest descent minimization of 1000 steps followed by 9000 step conjugate gradient minimizations at an ambient pressure of 1 bar and a constant temperature of 300 K. The step size was maintained at 1 fs. After those steps, the three-dimensional models were prepared using PyMOL Molecular Graphics System (Version 1.5.0.4, Schrödinger, LLC, New York, NY, USA) and Coot30,[23] based on the structure of human TRPM4[10] (PDB code: 5WP6).

2.10 | Statistics

Data are represented as the mean ± SEM. Sample distribution was tested for normality using D'Agostino & Pearson test in Prism 7.0 software (GraphPad Software Inc, USA). The unpaired two-tailed Student's test was used to analyze wild type and mutants with a probability value below 0.05 ($P < .05$) considered as significant. *P* values are given for each statistical comparisons in the figure panels. "n"-numbers are given as the number of investigated cells (patch-clamp) or transfections (western blot). The consistent results are confirmed by least two independent repeats of measurements.

3 | RESULTS

3.1 | K914R slows the gating properties of TRPM4 channel and increases membrane current without altering protein's expression

To study the functional consequences and explore possible disease related molecular mechanisms of the K914R mutation, we transiently expressed wild-type TRPM4 ($TRPM4^{wt}$) and $TRPM4^{K914R}$ in HEK293 cells and investigated their Ca^{2+}-dependent behavior with the Ca^{2+} uncaging approach described recently.[8] We found that trains of UV-flashes induced approximately three fold more membrane current in the $TRPM4^{K914R}$ mutant when compared to the $TRPM4^{wt}$ protein (455.9 ± 56.3 pA/pF, n = 11 vs 154.1 ± 13.0 pA/pF, n = 11, respectively, Figure 1A,B) while no significant change in $K_{D,Ca}$ was identified (Figure 1C). When analyzing their activation and deactivation properties, we noticed that the $TRPM4^{K914R}$ mutation displayed slower kinetics in both, activation (291.8 ± 37.2 ms (wt, n = 16) vs 585.8 ± 99.2 ms (mutation, n = 13); Figure 1D) and deactivation processes (2.2 ± 0.2 seconds (wt, n = 13) vs 6.7 ± 0.6 seconds (mutation, n = 14); Figure 1E). Expression differences were not the reason for the vastly different plasma membrane currents found, because our immunoblotting experiments indicated no significant difference between the expression of $TRPM4^{wt}$ and $TRPM4^{K914R}$ proteins on both, the global and the plasma membrane level (Figure 1F,G, respectively). These data indicated that the conservative substitution from lysine to arginine at position 914 in the S4-S5 linker severely affected the normal function of TRPM4 channels.

To further analyze the putative contribution of the K914R mutant to changes in ionic currents during human cardiac action potentials, we recorded action potentials from human-induced pluripotent stem cells-derived cardiac myocytes (hiPSC-CMs) with ventricular identity as described earlier[8] and used those voltage recordings as templates for action potential playback in HEK293 cells expressing $TRPM4^{wt}$ or $TRPM4^{K914R}$ channels (Figure 2A). UV-flash-mediated Ca^{2+} uncaging (Figure 2B) was triggered immediately following the onset of the action potential (Figure 2A, marked by the vertical dashed lines) to mimic the Ca^{2+} increase during a cardiac action potential. This experimental regime resulted in large and dynamic membrane currents that almost returned to baseline values between consecutive action potentials for the wt protein as shown by the black trace in Figure 2C. In contrast to that, the K914R mutant displayed a substantially distorted and increased the membrane current (red trace in Figure 2C). We compared the currents at the peak of the action potential (indicated by the labels above the action potentials in Figure 2A) and at full repolarization (labels below the action potentials in Figure 2A) in the panels Figure 2D,E, respectively. These data strongly suggest that once activated by Ca^{2+} $TRPM4^{K914R}$ generated excessive, accumulating membrane currents with diminished deactivation between consecutive human action potentials. Such persistent membrane currents may severely deform the shape of human action potentials, alter the diastolic membrane potential and in this way directly contribute to the pathology of human cardiac conduction diseases.

3.2 | K914G and K914E render TRPM4 non-functional

Amino acid K914 is located in the S4-S5 linker region (see Figure 3A), which was suggested as an important domain for

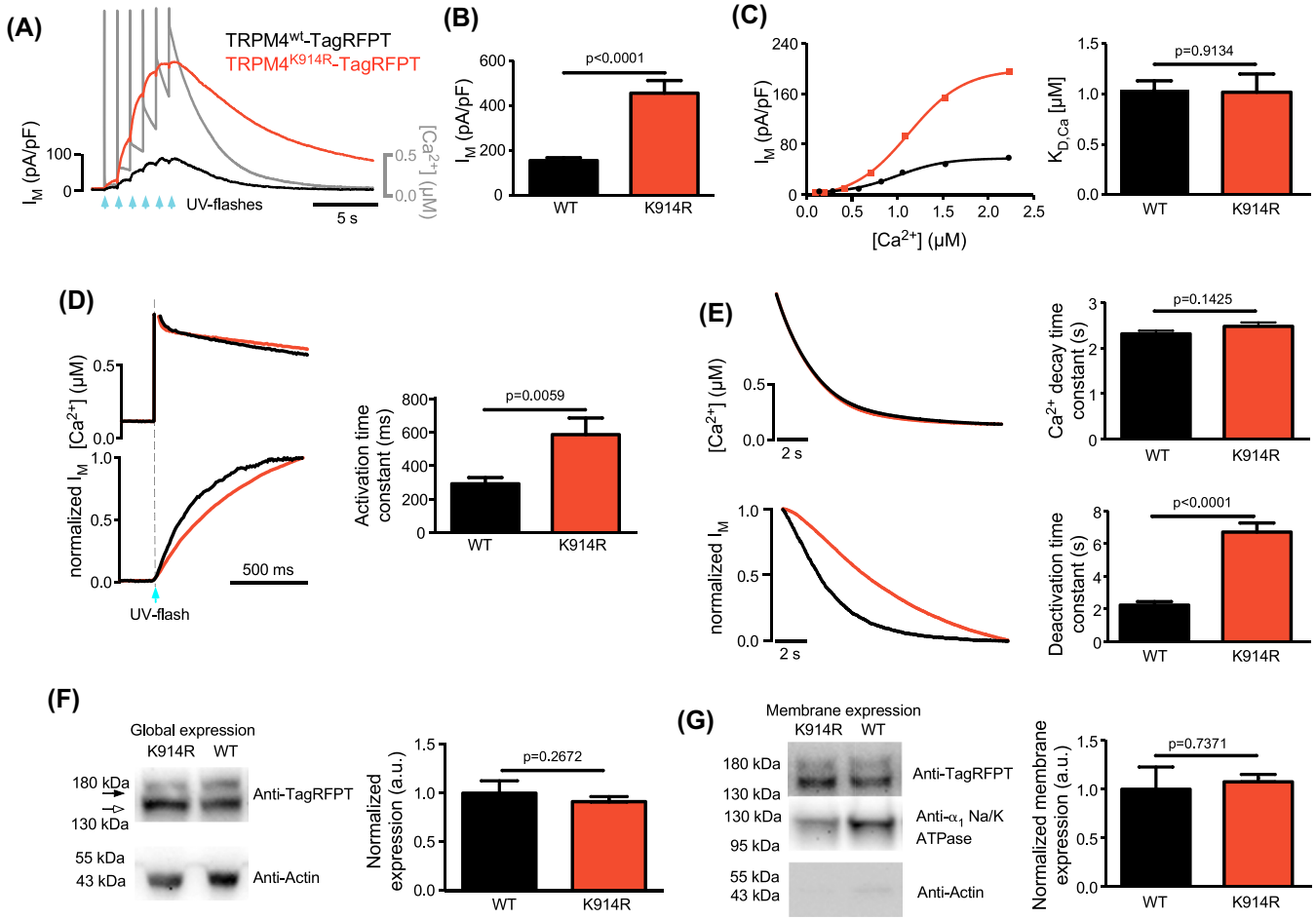

FIGURE 1 TRPM4^{K914R} slows Ca^{2+}-dependent channel gating and enhances membrane current without altering the protein's expression. A, Typical currents recorded in HEK293 cells transiently expressing TRPM4^{wt} (black) and TRPM4^{K914R} (red) as well as the Ca^{2+} concentration (gray) during a train of UV-flashes (turquoise triangles). B, Statistical analysis of the maximum membrane current density from TRPM4^{wt} and TRPM4^{K914R} (n = 11 cells for each group). C, Typical membrane vs Ca^{2+} relationships of TRPM4^{wt} and TRPM4^{K914R} (right) and statistical analysis (left) (n = 14 cells for TRPM4^{wt} and n = 10 cells for TRPM4^{K914R}). D, Typical normalized activation currents (lower left) activated by Ca^{2+} transients (upper left) induced by UV-flash and statistical analysis of activation time constants (right) (n = 16 cells for TRPM4^{wt} and n = 13 cells for TRPM4^{K914R}). E, Typical normalized deactivation currents (lower left) and statistical analysis of deactivation time constants (lower right) as well as the corresponding Ca^{2+} decay traces (upper left) and the decay time constants (upper right) (n = 13 cells for TRPM4^{wt} and n = 14 cells for TRPM4^{K914R}). F, Typical western blot of whole cell lysates of TRPM4^{wt} and TRPM4^{K914R} (left) as well as the statistical analysis (right) (n = 4 cultures for TRPM4^{wt} and n = 5 culture for TRPM4^{K914R}). G, Typical western blot of TRPM4^{wt} and TRPM4^{K914R} on the plasma membrane (left) and the statistical analysis (right) (n = 4 cultures for TRPM4^{wt} and n = 5 culture for TRPM4^{K914R}). Data information: In (B-G), data are presented as mean ± SEM. $^{**}P \leq .01$, $^{***}P \leq .001$ (Unpaired two-tailed Student's *t* test)

the function of TRP channels.[20] To further substantiate this role, we replaced the lysine, like arginine a positively charged basic amino acid by amino acids of distinct physicochemical properties, by glycine, the simplest nonpolar aliphatic amino acid, and glutamate, an acidic, negatively charged amino acid (Figure 3B), and expressed those TRPM4 variants in HEK293 cells. Neither the glycine nor the glutamate substitution was able to generate substantial membrane currents that were distinguishable from the background membrane current found in non-transfected HEK293 cells (Figure 3C). When we analyzed the expression and distribution of the TRPM4-TagRFPT variants in HEK293 cells and we verified both, ready expression of the protein indicated by the substantial TagRPFT fluorescence and strong plasma membrane decoration (Figure 3D).

Following from these unexpected findings, we investigated the putative molecular mechanism for that behavior. Based on the electron cryo-microscopy structure of TRPM4 reported recently,[12] residue K914 within the S4-S5 linker interacts with residues in the TRPM Homology Region (MHR) 4 domain (Q673, T677, W680 and W681) and the TRP helix (W1058, K1059 and R1062) as depicted in Figure 4A. The residue K914 (positive charge) interacts with T677 through hydrogen bonds and with all other amino acids via hydrophobic interactions to form a stable functional interdomain interface (Figure 4A). Molecular dynamic simulation can

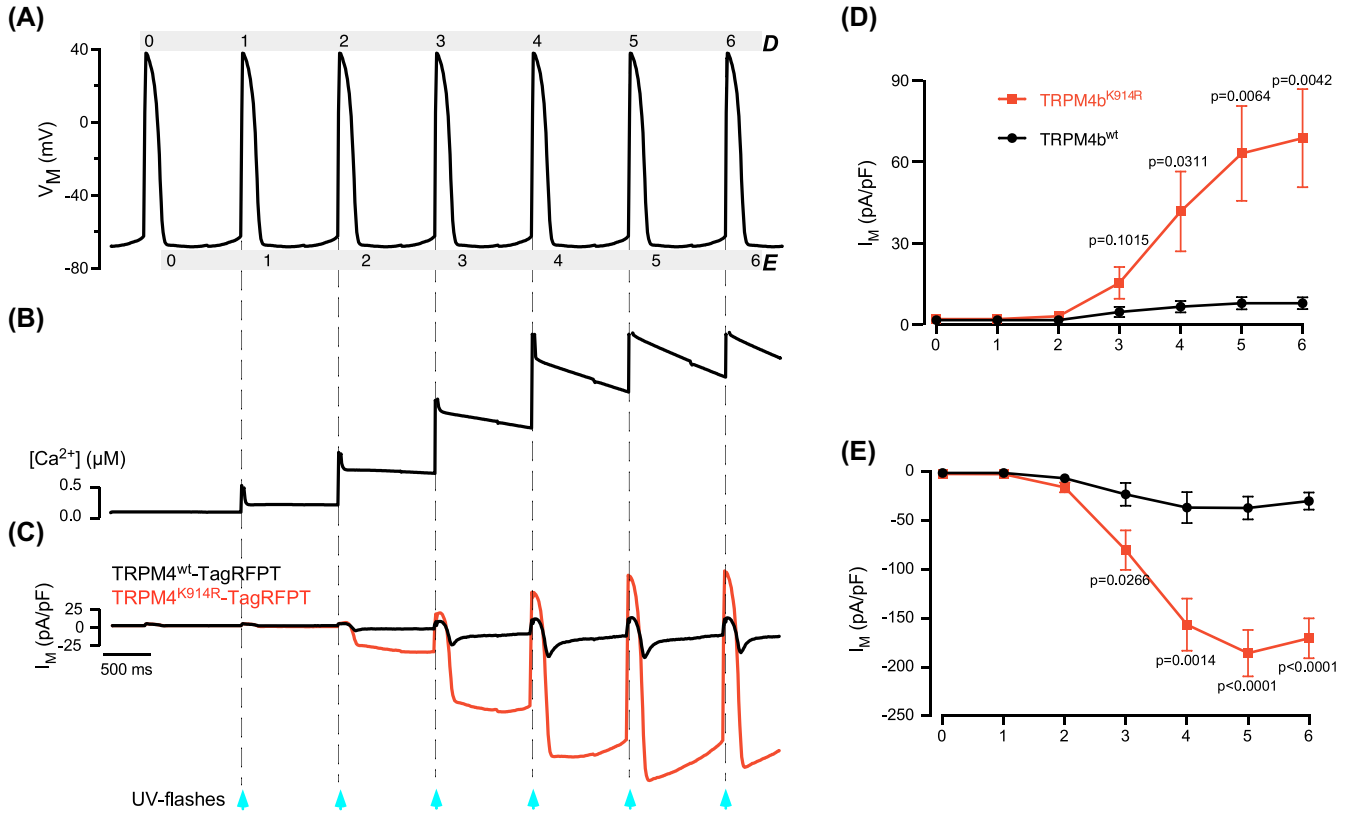

FIGURE 2 TRPM4^{K914R} generates excessive membrane currents during human ventricular action potentials. A, Action potentials recorded from the ventricular-like human-induced pluripotent stem cell-derived cardiac myocyte (hips-CM). B, Intracellular Ca^{2+} concentration during the experimental regime. C, TRPM4^{wt} (black) and TRPM4^{K914R} (red) mediated membrane current traces resulting from the command voltage shown in (A) and Ca^{2+} concentration (B). D, Statistical analysis of the currents in (C). Currents were probed at the points indicated by the numbers above the action potentials in (A) (n = 9 cells for both groups). E, Statistical analysis of the currents in (C). Currents were probed at the points indicated by the numbers below the action potentials (full repolarization) in (A) (n = 9 cells for both groups). Data information: In (D-E), data are presented as mean ± SEM. *$P \leq .05$, **$P \leq .01$, ****$P \leq .0001$ (Unpaired two-tailed Student's *t* test)

calculate the total energy of given protein structures.[24] We found that the energy contents of the crystal structures derived for the mutated TRPM4 variants were similar to that of the wild-type human TRPM4 structure (PDB code: 5WP6). This indicated an equal stability and rationality between the TRPM4^{wt} structure and those of the mutant proteins (Table S1). In the human K914R mutant, arginine apparently snaps into a molecular pocket formed by the MHR4 and TRP helix due to its more spacious guanidinium group providing three asymmetrical nitrogen atoms. As a consequence of that it may deform the S4-S5 linker leading to increased interactions with additional amino acids (hydrophobic interactions with W680, W681, P689, I690, W691, W1058, and R1062 and hydrogen bonds with T677 and T687). These extra interactions appear to lock the S4-S5 linker in a rigid unzipped position (Figure 4B). With glycine at site 914, the existing interactions were lost, which may disrupt the function of the TRPM4 channel (Figure 4C). In comparison to the wt lysine (K914), glutamate enables an increased number of hydrogen bonds and less hydrophobic interactions with its surrounding amino acids (Q673, R1062, and K1059: hydrogen bonds; W680, W681 T677, and W1058: hydrophobic interaction). This situation might "lock" the entire domain structure in this "zipped" position (Figure 4D) to render the channel non-functional. Based on these analyses, we propose that alterations of the amino acid at position 914 might render TRPM4 mal-functional or non-functional due to a disruption or modulation of the interaction between the S4-S5 linker and surrounding domains such as the MHR4 domain and the TRP helix.

3.3 | An artificial amino acid exchange (R1062Q) in the TRP box offsets the malfunction caused by the K914R mutation

TRPC, TRPM, and TRPV channels contain a TRP domain—a ~25 residue conserved sequence- following the S6 segment at the C-terminal end of the proteins. Therein, the most conserved TRP box motif consists of six amino acids (EWKFAR) in the TRPC subfamily or five amino acids (WKFQR) in the TRPM subfamily. In TRPV4, the S4-S5

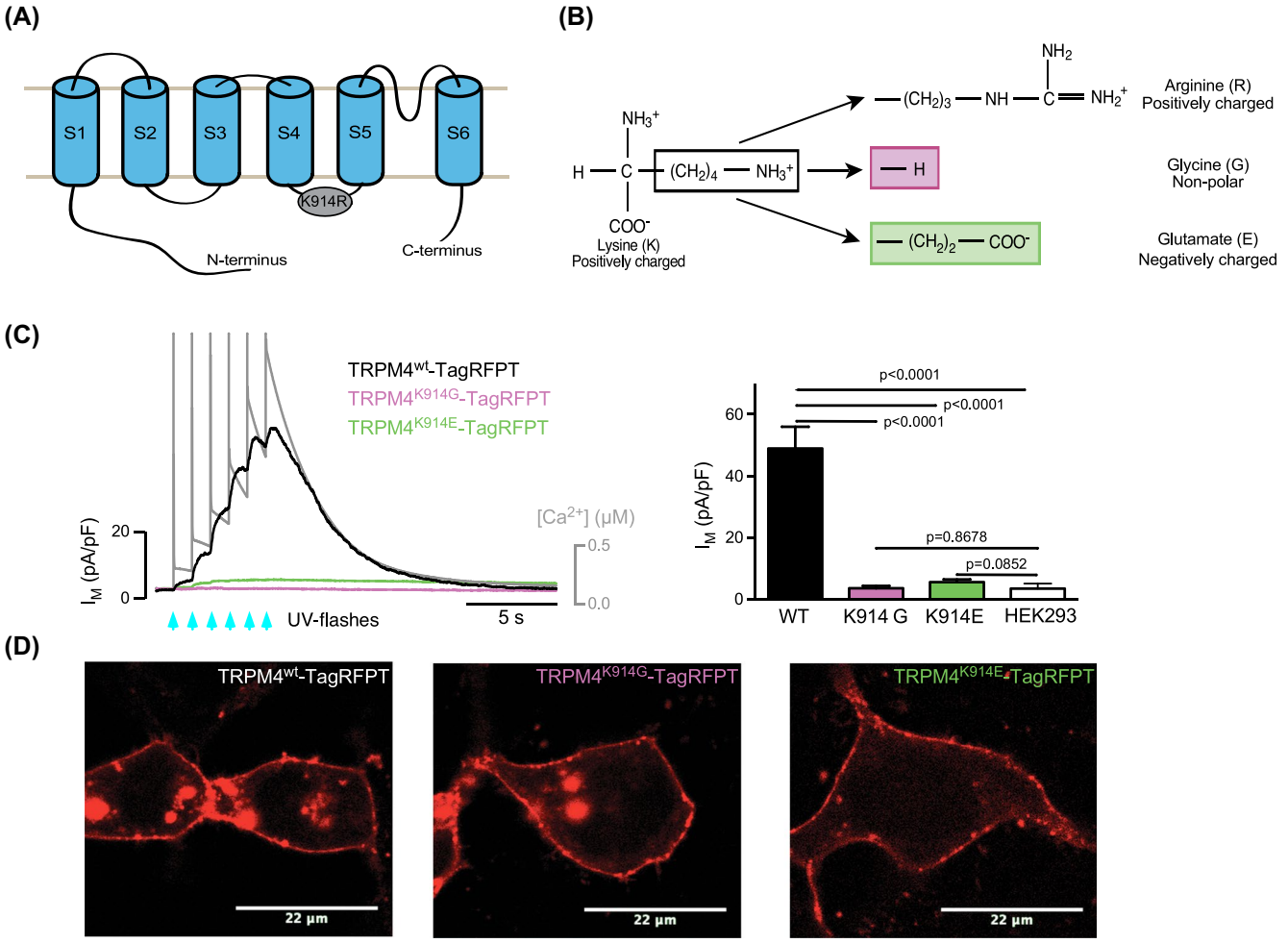

FIGURE 3 TRPM4^{K914G} and TRPM4^{K914E} variants render the channel non-functional. A, Schematic representation of TRPM4's membrane topology indicating the position of human mutation K914R. B, Structure and properties of TRPM4^{wt}, TRPM4^{K914R}, TRPM4^{K914G}, and TRPM4^{K914E}. Color coding indicating by the color of rectangles. C, Currents of TRPM4 variants activated by a series of UV-flash-induced Ca^{2+} jumps (gray, left) and the statistical analysis of the membrane current density (right) (n = 11 cells for wt, n = 8 cells for K914G, n = 10 for K914E, and n = 8 for naíve HEK cells). D, Confocal section through the middle of HEK293 cells expressing TRPM4 variants as indicated. Data information: In (C), data are presented as mean ± SEM. ***$P \leq .001$, ****$P \leq .0001$ (Unpaired two-tailed Student's *t* test)

linker has been suggested to interact with the TRP domain to modulate the channel's gating kinetics.[16] Based on the electro cryo-microscopy structure of the TRPM4 channel, the hydrophobic interactions between the K914 in S4-S5 linker and the three residues (W1058, K1059, and R1062) in the TRP box (Figure S2) may suggest similar interactions between S4-S5 linker and TRP domain for the TRPM4 channel. Nilius and co-workers reported an increased deactivation of the TRPM4 channel after introducing the R1062Q mutation[25] and we wondered whether this mutation (R1062Q) in the TRP box is able to rescue the current phenotype of the TRPM4^{K914R} mutation.

We characterized the behavior of TRPM4^{R1062Q} (Figure 5) and found that TRPM4^{R1062Q} displayed a decreased membrane current (52.1 ± 7.6 pA/pF, n = 14, Figure 5A,B) when compared to that of TRPM4^{wt} (115.1 ± 20.4 pA/pF, n = 12) without altering the protein's global and plasma membrane expression (Figure 5F,G, respectively). No significant difference in the current's Ca^{2+} sensitivity was detected (Figure 5C) but membrane currents of TRPM4^{R1062Q} were characterized by a faster activation and deactivation time constants (133.0 ± 9.5 ms, n = 9 and 2.2 ± 0.1 seconds, n = 18, respectively), when compared to the wt channels (211.7 ± 21.7 ms, n = 12 and 3.0 ± 0.2 seconds, n = 14) (Figure 5D,E).

We then tested the double mutant TRPM4$^{K914R+R1062Q}$ and found that it could indeed partially offset altered parameters of the TRPM4^{K914R} mutation. As shown in Figure 6A,B, the membrane current was reduced by 26% (from 199.8 ± 17.2 pA/pF, n = 13 in TRPM4^{K914R} to 147.2 ± 14.1 pA/pF, n = 14 in TRPM4$^{K914R+R1062Q}$) while the $K_{D,Ca}$ remained unchanged (Figure 6C). Notably, for TRPM4$^{K914R+R1062Q}$ the activation (Figure 6D) and deactivation (Figure 6E) became faster than that of the human single mutation TRPM4^{K914R} (493.6 ± 42.7 ms, n = 11 and 3.1 ± 0.1 seconds, n = 13 vs

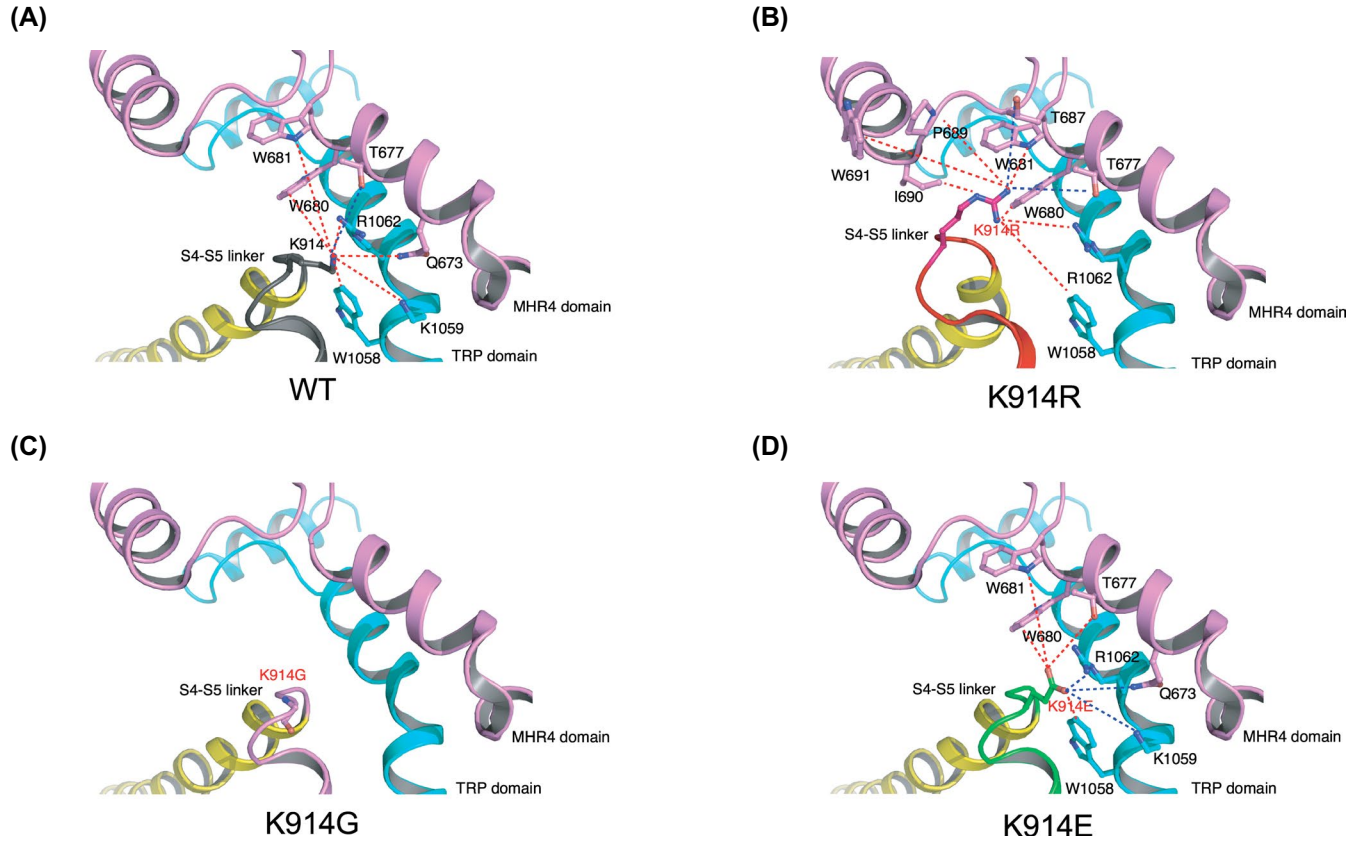

FIGURE 4 The amino acid at position 914 modifies the interface between the S4-S5 linker, TRP domain, and MHR4 domain in the TRPM4 protein. A-D, Models of the S4-S5 linker, TRP domain and MHR4 domain interface calculated for various amino acids at position 914: lysine in the wt protein (A), arginine in the K914R mutation (B), glycine in the K914G mutation (C) and glutamic acid in the K914E mutation (D). Dashed lines indicate putative coordinating amino acid interactions (red dashed lines: hydrophobic interactions; blue dashed lines: hydrogen bonds). Structures were derived from the previously solved structure of the human TRPM4 channel (PDB code 5WP6)

654.3 ± 46.4 ms, n = 12 and 7.4 ± 0.4 seconds, n = 14). Western blot analysis showed that for both proteins, the global as well as the plasma membrane expression were unchanged (Figure 6F,G). Nevertheless, we observed that the $TRPM4^{K914R+R1062Q}$ channel still exhibited the increased current density, the slower activation, and deactivation kinetics reminiscence of the K914R single mutation when compared to $TRPM4^{wt}$ (Figure S1). These findings indicate that the introduced mutation R1062Q in the TRP box could partially offset the aberrant functions resulting from the human mutation K914R in the S4-S5 linker.

3.4 | The interface between the S4-S5 linker, the MHR4 domain, and the TRP domain modulate TRPM4's properties

The electron cryo-microscopy structure of TRPM4 channel[10] suggests that in the human $TRPM4^{wt}$ channel hydrophobic interactions can be formed between K914 in the S4-S5 linker and R1062 in the TRP box. We suggest that these interactions represent the overall forces for a stable protein structure and maintain a proper distance between the S4-S5 linker and TRP domain (Figure 7A) that warrant normal TRPM4 gating (Figure 1, in black). The switch from the positively charged arginine (R) to the polar and uncharged glutamine (Q) at position 1062 induces H-bonds between $lysine^{914}$ and $glutamine^{1062}$. This stronger interaction reduces the critical distance between the TRP domain and the S4-S5 linker and lock them in a zipped position when compared to the wt situation (compare Figure 7A,B) resulting in an altered function with speed-up activation and deactivation kinetics (Figure 5 in brown). In contrast, the hydrophobic interaction due to the electrostatic force between $arginine^{914}$ and $arginine^{1062}$ in $TRPM4^{K914R}$ mutant results in a repulsion between the S4-S5 linker and the TRP domain (Figure 7C). Consequently, the distance between these two domains widens and unzipped the S4-S5 linker causing a gain-of-function with slowed down activation and inactivation kinetics. Eventually, H-bonds between $arginine^{914}$ and $glutamine^{1062}$ in the $TRPM4^{K914R+R1062Q}$ variant partially offset the repelling forces modeled for the $TRPM4^{K914R}$ mutant and close and zip the gap between the S4-S5 linker and the TRP domain (Figure 7D) resulting

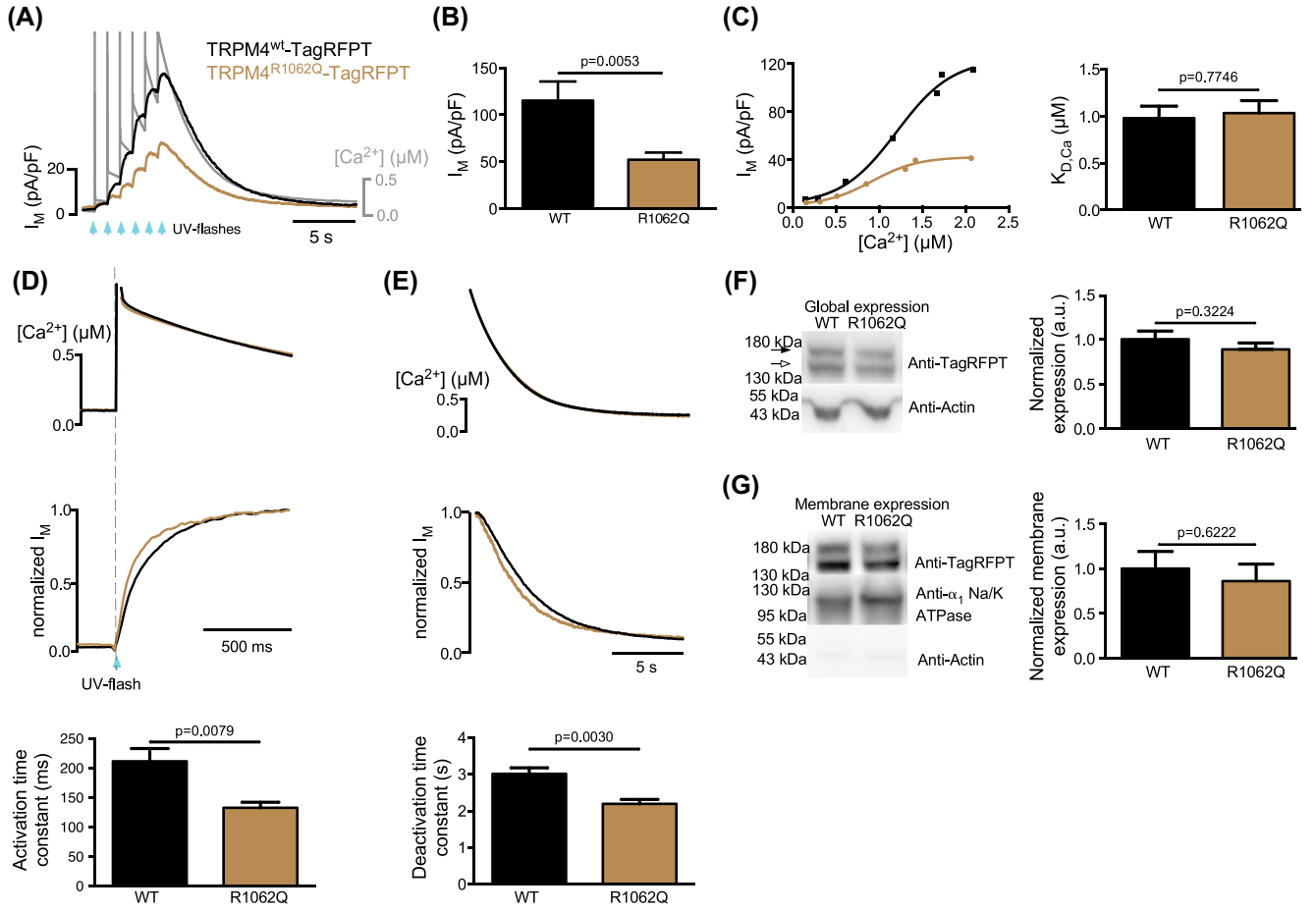

FIGURE 5 Amino acid at position 1062 in the TRP domain modulates TRPM4's properties. A, Typical currents of cells transiently expressing TRPM4^{wt} (black) and TRPM4^{R1062Q} (brown) and the intracellular Ca^{2+} concentrations (gray) during a series of UV-flashes. B, Statistical analyses of the maximum membrane current densities of TRPM4^{wt} and TRPM4^{R1062Q} (n = 12 cells and n = 14 cells, respectively). C, The current vs Ca^{2+} concentration relationship (left) and statistical analyses (right) (n = 11 cells for each group). D, Normalized activation currents (middle) elicited by a Ca^{2+} jump (top) and the statistical analyses of activation time constants (bottom) (n = 9 cells for TRPM4^{wt} and n = 12 cells for TRPM4^{R1062Q}). E, Normalized deactivation currents (middle) as well as the Ca^{2+} decay traces (top) and statistical analyses of deactivation time constants (bottom) (n = 14 cells for TRPM4^{wt} and n = 18 cells for TRPM4^{R1062Q}). F, Western blot of whole cell lysates of TRPM4^{wt} and TRPM4^{R1062Q} (left) and the statistical analyses (right) (n = 4 cultures for TRPM4^{wt} and n = 5 cultures for TRPM4 ^{R1062Q}). G, Western blot of plasma membrane protein of TRPM4^{wt} and TRPM4^{R1062Q} (left) and the statistical analyses (right) (n = 4 cultures for TRPM4^{wt} and n = 5 cultures for TRPM4 ^{R1062Q}). Data information: In (B-G), data are presented as mean ± SEM. $^{**}P \leq .01$ (Unpaired two-tailed Student's *t* test)

in a shift of the channel's behavior toward "wt behavior" (see Figure 6). Residues involved in the intramolecular interface of S4-S5 linker, TRP domain, and MHR4 domain are shown in Figure S2. Modeling energy evaluations are shown in Table S1. These structural modeling results offer a molecular mechanism for the channel's properties presented above and strongly suggest a very important interaction between the S4-S5 linker region and the TRP domain for the proper gating of the TRPM4 channel.

4 | DISCUSSION

In the present study, we revealed that the TRPM4^{K914R} mutant found in patients with atrioventricular-block displays aberrant behavior in Ca^{2+}-induced gating with 2 to 3-fold slowed-down Ca^{2+}-dependent activating and deactivating kinetics and a substantially increased membrane current density. The increased membrane current was not a result of an altered global or plasma membrane protein expression when compared to the wt protein suggesting that it might be a direct result of the altered gating kinetics rather than an increased protein accumulation.[2] To gain additional insight into the putative contribution of this mutation to aberrant cardiac electrophysiology, we recorded native action potentials from ventricular-like hiPSC-CMs and used these voltage traces as templates in action potential play-back experiments. These studies demonstrate K914R's potential in substantially altering the shape and time course of human action potentials and thus suggests a novel disease mechanism

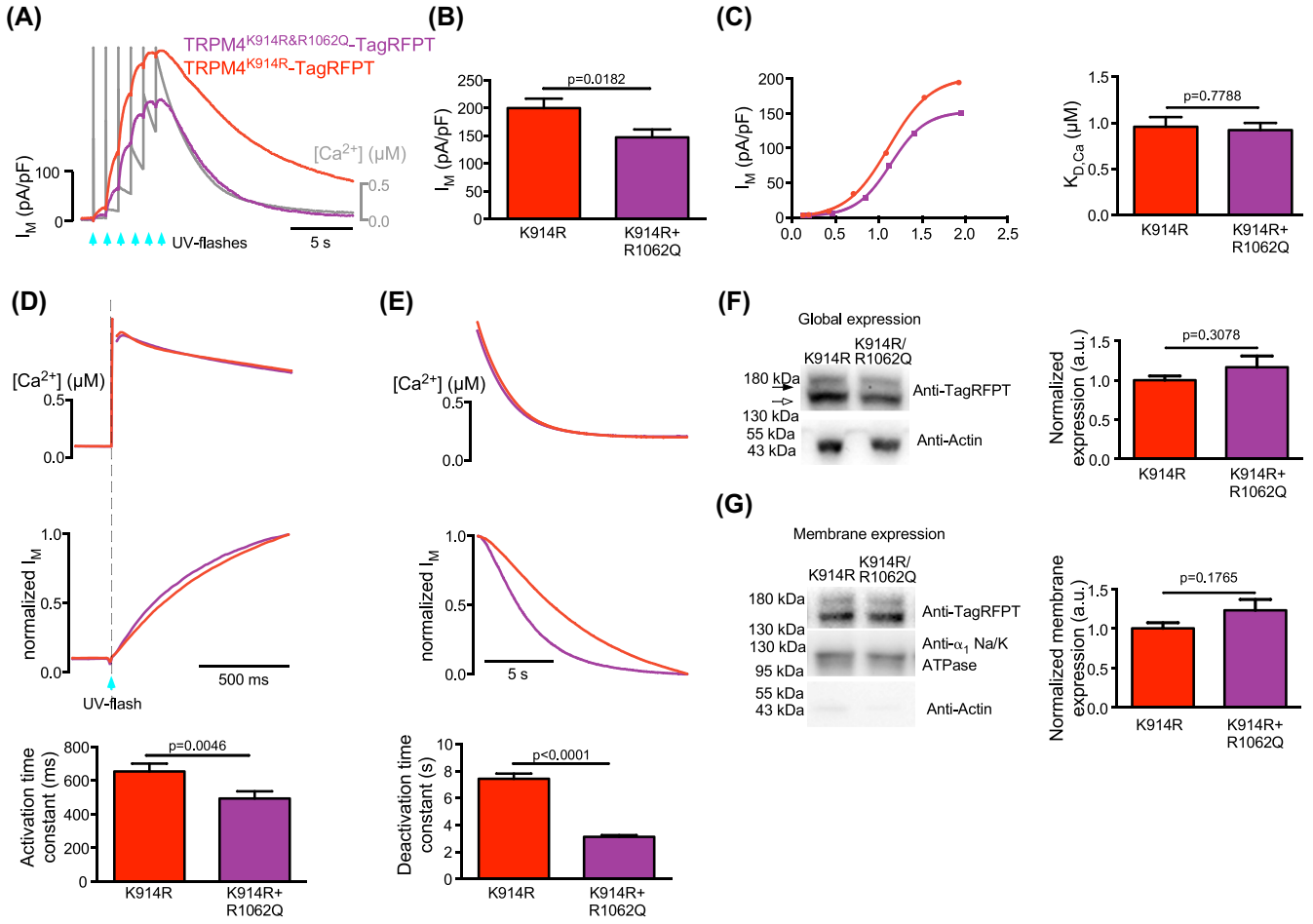

FIGURE 6 R1062Q partially offsets the aberrant properties of the K914R mutation in TRPM4. A, Typical currents of cells transiently expressing TRPM4^{K914R} (red) and TRPM4^{R1062Q} (magenta) and the intracellular Ca^{2+} concentrations (gray) during a series of UV-flashes. B, Statistical analyses of the maximum membrane current densities of TRPM4^{K914R} and TRPM4$^{K914R+R1062Q}$ (n = 13 cells and n = 14 cells, respectively). C, The current vs Ca^{2+} concentration relationship (left) and statistical analyses (right) (n = 10 cells for TRPM4^{K914R} and n = 14 cells for TRPM4$^{K914R+R1062Q}$). D, Normalized activation currents (middle) elicited by UV-flash-induced Ca^{2+} jumps (top) and the statistical analyses of activation time constants (bottom) (n = 12 cells for each group). E, Normalized deactivation currents (middle) as well as the Ca^{2+} decay traces (top) and statistical analyses of deactivation time constants (bottom) (n = 14 cells for TRPM4^{K914R} and n = 13 cells for TRPM4$^{K914R+R1062Q}$). F, Western blot of whole cell lysates of TRPM4^{K914R} and TRPM4$^{K914R+R1062Q}$ (left) and the statistical analyses (right) (n = 4 cultures for each group). G, Western blot of plasma membrane protein of TRPM4^{K914R} and TRPM4$^{K914R+R1062Q}$ (left) and the statistical analyses (right) (n = 4 cultures for each group). Data information: In (B-G), data are presented as mean ± SEM. *$P \leq .05$, ***$P \leq .001$ (Unpaired two-tailed Student's *t* test)

for TRPM4-dependent AV-blocks in patients: aberrant Ca^{2+}-dependent gating through intramolecular domain zipping and unzipping.

For more than a decade the importance of the S4-S5 linker in the control of voltage-dependent gating of TRPM4 has been suggested.[26] TRPM4 and its related proteins TRPM2, TRPM5, and TRPM8, all contain two basic amino acids in this S4-S5 linker. Neutralizing the positively charged residues (R842 and K856) in TRPM8 shift its voltage dependence.[27] Our data provides direct functional evidence that the S4-S5 linker is a modulator of TRPM4's Ca^{2+}-dependent gating (Figure 1) highlighting its possible importance for TRPM4's behavior. To investigate the role of this region in greater detail, we changed the positively charged residue lysine to the nonpolar residue glycine and to the negatively charged glutamate. Both variants lacked any Ca^{2+}-dependent membrane currents. Two possible mechanisms can be envisaged. Either direct Ca^{2+}-binding pocket of TRPM4 or indirect Ca^{2+}-dependent gating of TRPM4 is modified by these mutations. A previous report investigating the E1068Q amino acid exchange within the TRP domain depicted a reduced Ca^{2+}-sensitivity of the TRPM4 channel because of its steric proximity to the path leading to the putative Ca^{2+}-binding sites from the cytoplasmic space.[12] Four amino acids have been proposed to coordinate Ca^{2+} binding (glutamate^{828}, glutamine^{831} from S2 and asparagine^{865}, aspartate^{868} from S3).[12] Because these coordinating amino acids appear further away from the S4-S5 linker and the mutation TRPM4^{K914R} did not affect the Ca^{2+} sensitivity of the TRPM4 channel (Figure 1C), we suggest that position 914 is not a site directly

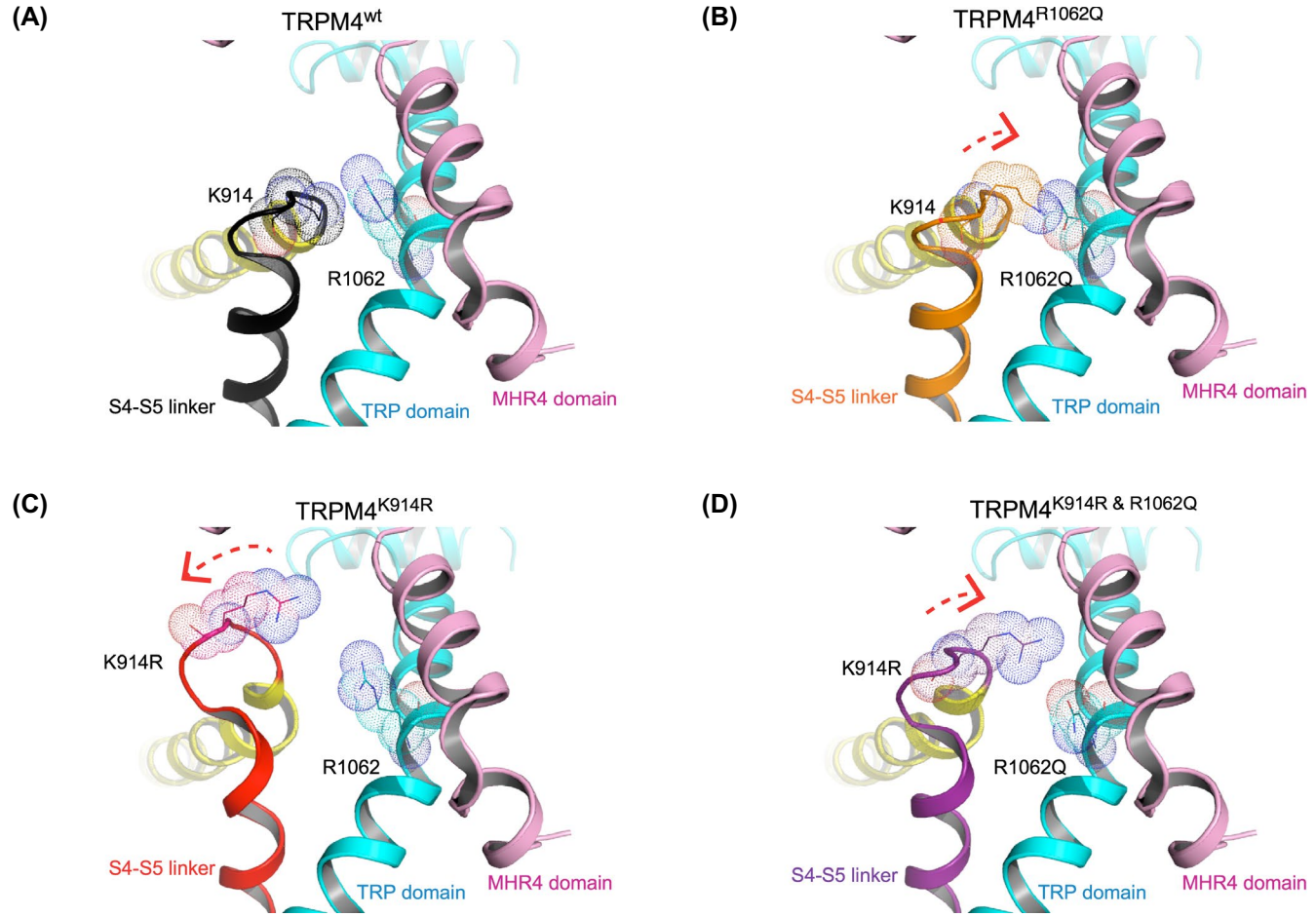

FIGURE 7 The interface between the S4-S5 linker, the TRP domain, and the MHR4 domain modulates TRPM4's functions. A-D, Models of the S4-S5 linker, TRP domain, and MHR4 domain interface calculated for various amino acids at position 914 and 1062 (as indicated). Dotted volumes indicate the approximate volume occupied by the indicated amino acids. The red arrows indicate contraction or widening of the S4-S5 linker—TRP domain interface. Structures were derived from the previously solved structure of the human TRPM4 channel (PDB code 5WP6). S4-S5 linker is highlighted with black ($TRPM4^{wt}$), red ($TRPM4^{K914R}$), orange ($TRPM4^{R1062Q}$), and purple ($TRPM4^{K914R+R1062Q}$), respectively

modulating TRPM4's Ca^{2+}-binding pocket. As reported for the TRP family in general, the S4-S5 linker plays a crucial role in the channel's gating kinetics through an interaction with the TRP domain.[16,20] A "conformational" changes induced by peptides targeting TRP domain in TRPV1 channel has been reported to lead to gate opening.[28] In the structure of the TRPM4 channel, the S4-S5 linker indeed seems to directly interact with the TRP domain and the MHR4 domain.[10-12] Our molecular modeling of the amino acid substitutions suggests an alteration of the nanoscopic interface's stability and zipping state (Figure 4). This may render the channel non-functional by destroying essential interactions between the internal domains (S4-S5 linker, MHR4, and TRP domain) deteriorating the gating kinetics, specifically channel opening and closing but leaving Ca^{2+}-binding sites untouched. Even though we did not observe any changes in the Ca^{2+} sensitivity of the TRPM4 variants, it has to be realized that the Ca^{2+} binding process of the TRPM4 protein is modulated by multiple factors, such as ATP and PKC-dependent phosphorylation.[29] Ca^{2+}- calmodulin binding sites at the C terminus have been reported to regulate the Ca^{2+} sensitivity of TRPM4 channels.[29] In the structure of TRPM4, residues surrounding the putative Ca^{2+}-binding sites might also contribute to the coordination of Ca^{2+} binding.[12] Thus, it is still uncertain whether the unchanged Ca^{2+} sensitivity observed in our results is directly due to an unaltered Ca^{2+} binding process. Alternatively, the mutations might exert a compensatory effect on the regulation processes or the spatial arrangement within the molecule itself resulting in an apparently unaltered Ca^{2+} sensitivity.

In general, the TRP domain is considered important for very diverse processes such as channel gating and allosteric modulation.[30-32] In the TRPM4 channel, the TRP domain displays extensive interactions with its neighboring domains.[11,12] The interaction between the TRP domain and the N-terminal domain is mediated by five residues (K1059, R1062, R1067, L1056, and Y1063) and four residues (L655, Q673, T677, and R664), respectively.[11] The TRP domain putatively interacts with the S4-S5 linker through hydrogen bridges similar to those found in the TRPV1 and TRPA1 proteins.[33-35] In particular,

the N913 in the S4-S5 linker contacts R1062 of the TRP domain via hydrogen bonds.[11] The invariant residue W1058 in the TRP domain is embraced by the S4-S5 linker, forming a possible hydrogen bond with T911 in the S4-S5 linker.[10] In our study, we confirmed the importance of R1062 in that a substitution of the arginine with glutamine caused aberrant TRPM4 behavior characterized by accelerated Ca^{2+}-dependent activation and deactivation kinetics and a reduced membrane current density (loss-of-function) (Figure 5). Interestingly, molecular modeling indicated that R1062 and K914 share the same interaction interface in the TRPM4 molecule and possibly even interact directly. We, therefore, investigated whether the R1062Q variant might actually be efficient in offsetting the effects seen in the K914R variant. We found that indeed the slowed down gating kinetics and the increased membrane current density could—at least partially—be "compensated" for by the R1062Q amino acid exchange. These findings strongly supported our notion that both amino acids K914 and R1062 not only share the same nanodomain and interact but that this particular interaction interface might be a critical determinant for TRPM4's Ca^{2+}-dependent gating (Figure 6). A detailed analysis of our molecular modeling of this interaction region indeed revealed a possible molecular mechanism modulating the channel's behavior. It appears that due to the residues' interactions, maintaining a precise distance between the S4-S5 linker and the TRP domain is essential for a normal function of the TRPM4 channel. Stronger interactions in the R1062Q variant appear to close the gap between these structures, lock them in a zipped configuration and thus cause a loss of function while a weaker interaction as proposed for the K914R variant widens the S4-S5 linker—TRP domain gap (unzipping) and causes gain-of-function in the TRPM4 protein. Moreover, in the K914R variant the S4-S5 linker appears to be locked in this "open" or unzipped position. Supporting this notion, the double amino acid exchange in the $TRPM4^{K914R+R1062Q}$ variant results in a reduced repulsion between these domains when compared to the human mutation $TRPM4^{K914R}$ and may thus partially compensate the kinetic alterations resulting from the latter amino acid exchange (Figures 7 and S2).

In conclusion, our study reveals that the mutation $TRPM4^{K914R}$ identified in patients with cardiac conduction diseases such as AV-block mediates a malfunctional TRPM4 channel that can generate excessive membrane current during cardiac action potentials and the accompanying Ca^{2+} transients. Furthermore, we identified the underlying molecular mechanism, the intimate interface between the S4-S5 linker and the TRP domain is at the center of this malfunction. Amino acid exchanges that weaken (unzipping) this interaction result in slowed-down Ca^{2+}-dependent activation and deactivation kinetics associated with substantially enhanced membrane currents, while those strengthening the interaction (zipping) cause augmented kinetics and reduced membrane currents. Human mutations affecting this important intramolecular nanodomain can, therefore, alter the cardiac myocyte's electrophysiological properties and can cause severe conduction inheritable diseases. Deeper insights into such molecular mechanisms by our study may offer new pharmacological targets for novel disease management.

COMPETING INTEREST

The authors declare no competing interest.

ACKNOWLEDGMENTS

Part of this work was funded by the SFB TRR 152 (Deutsche Forschungsgemeinschaft [DFG]) to WX, AM, K.-LL, VF, and PL. HW is a recipient of an Alexander von Humboldt research scholarship in the Flockerzi lab. Open access funding enabled and organized by Projekt DEAL.

AUTHOR CONTRIBUTIONS

W.Xian & P.Lipp designed research and wrote the manuscript. W.Xian & H. Wang performed research. W.Xian, H. Wang, A.Moretti, K.-L. Laugwitz, V. Flockerzi & P.Lipp analyzed results and data. A.Moretti & K.-L. Laugwitz contributed research material.

REFERENCES

1. Nilius B, Prenen J, Droogmans G, et al. Voltage dependence of the Ca2+-activated cation channel TRPM4. *J Biol Chem*. 2003;278:30813-30820.
2. Kruse M, Schulze-Bahr E, Corfield V, et al. Impaired endocytosis of the ion channel TRPM4 is associated with human progressive familial heart block type I. *J Clin Investig*. 2009;119:2737-2744.
3. Liu H, Zein EL, Kruse M, et al. Gain-of-function mutations in TRPM4 cause autosomal dominant isolated cardiac conduction disease. *Circ Cardiovasc Genet*. 2010;3:374-385.
4. Stallmeyer B, Zumhagen S, Denjoy I, et al. Mutational spectrum in the Ca2+-activated cation channel gene TRPM4 in patients with cardiac conductance disturbances. *Hum Mutat*. 2011;33:109-117.
5. Liu H, Chatel S, Simard C, et al. Molecular genetics and functional anomalies in a series of 248 Brugada cases with 11 mutations in the TRPM4 channel. *PLoS One*. 2013;8:e54131.
6. Bianchi B, Ozhathil LC, Medeiros-Domingo A, Gollob MH, Abriel H. Four TRPM4 cation channel mutations found in cardiac conduction diseases lead to altered protein stability. *Front Physiol*. 2018;9:873-911.
7. Wang H, Xu Z, Lee BH, et al. Gain-of-function mutations in TRPM4 activation gate cause progressive symmetric erythrokeratodermia. *J Invest Dermatol*. 2019;139:1089-1097.
8. Xian W, Hui X, Tian Q, et al. Aberrant deactivation-induced gain of function in TRPM4 mutant is associated with human cardiac conduction block. *Cell Rep*. 2018;24:724-731.
9. Guo J, She J, Zeng W, Chen Q, Bai X-C, Jiang Y. Structures of the calcium-activated, non-selective cation channel TRPM4. *Nature*. 2017;552:205-209.
10. Winkler PA, Huang Y, Sun W, Du J, Lü W. Electron cryo-microscopy structure of a human TRPM4 channel. *Nature*. 2017;552:200-204.
11. Duan J, Li Z, Li J, et al., Structure of full-length human TRPM4. *Proc Natl Acad Sci USA*. 2018;115:2377-2382.

12. Autzen HE, Myasnikov AG, Campbell MG, Asarnow D, Julius D, Cheng Y. Structure of the human TRPM4 ion channel in a lipid nanodisc. *Science*. 2018;359:228-232.
13. Long SB, Campbell EB, Mackinnon R. Voltage sensor of Kv1.2: structural basis of electromechanical coupling. *Science*. 2005;309:903-908.
14. Cao E, Liao M, Cheng Y, Julius D. TRPV1 structures in distinct conformations reveal activation mechanisms. *Nature*. 2013;504:113-118.
15. Teng J, Loukin SH, Anishkin A, Kung C. A competing hydrophobic tug on L596 to the membrane core unlatches S4–S5 linker elbow from TRP helix and allows TRPV4 channel to open. *Proc Natl Acad Sci USA*. 2016;113:11847-11852.
16. Teng J, Loukin SH, Anishkin A, Kung C. L596–W733 bond between the start of the S4–S5 linker and the TRP box stabilizes the closed state of TRPV4 channel. *Proc Natl Acad Sci USA*. 2015;112:3386-3391.
17. Lin Z, Chen Q, Lee M, et al. Exome sequencing reveals mutations in TRPV3 as a cause of Olmsted syndrome. *Am J Hum Genet*. 2012;90:558-564.
18. Kremeyer B, Lopera F, Cox JJ, et al. A gain-of-function mutation in TRPA1 causes familial episodic pain syndrome. *Neuron*. 2010;66:671-680.
19. Zíma V, Witschas K, Hynkova A, Zímová L, Barvík I, Vlachova V. Structural modeling and patch-clamp analysis of pain-related mutation TRPA1-N855S reveal inter-subunit salt bridges stabilizing the channel open state. *Neuropharmacology*. 2015;93:294-307.
20. Hofmann L, Wang H, Zheng W, et al. The S4–S5 linker—gearbox of TRP channel gating. *Cell Calcium*. 2017;67:156-165.
21. Ho SN, Hunt HD, Horton RM, Pullen JK, Pease LR. Site-directed mutagenesis by overlap extension using the polymerase chain reaction. *Gene*. 1989;77:51-59.
22. Chen Z, Xian W, Bellin M, et al. Subtype-specific promoter-driven action potential imaging for precise disease modelling and drug testing in hiPSC-derived cardiomyocytes. *Eur Heart J*. 2016;38:292-301.
23. Emsley P, Lohkamp B, Scott WG, Cowtan K. Features and development of Coot. *Acta Crystallogr D Biol Crystallogr*. 2010;66:486-501.
24. Patodia S, Bagaria A, Chopra D. Molecular dynamics simulation of proteins: a brief overview. *J Phys Chem Biophys*. 2014;4:1-4.
25. Nilius B, Mahieu F, Prenen J, et al. The Ca2+-activated cation channel TRPM4 is regulated by phosphatidylinositol 4,5-biphosphate. *EMBO J*. 2006;25:467-478.
26. Nilius B, Vennekens R. From cardiac cation channels to the molecular dissection of the transient receptor potential channel TRPM4. *Pflugers Arch*. 2006;453:313-321.
27. Voets T, Owsianik G, Janssens A, Talavera K, Nilius B. TRPM8 voltage sensor mutants reveal a mechanism for integrating thermal and chemical stimuli. *Nat Chem Biol*. 2007;3:174-182.
28. Valente P, Fernández-Carvajal A, Camprubí-Robles M, et al. Membrane-tethered peptides patterned after the TRP domain (TRPducins) selectively inhibit TRPV1 channel activity. *FASEB J*. 2011;25:1628-1640.
29. Nilius B, Prenen J, Tang J, et al. Regulation of the Ca2+ sensitivity of the nonselective cation channel TRPM4. *J Biol Chem*. 2005;280:6423-6433.
30. Gregorio-Teruel L, Valente P, González-Ros JM, Fernández-Ballester G, Ferrer-Montiel A. Mutation of I696 and W697 in the TRP box of vanilloid receptor subtype I modulates allosteric channel activation. *J Gen Physiol*. 2014;143:361-375.
31. García-Sanz N, Valente P, Gomis A, et al. A role of the transient receptor potential domain of vanilloid receptor I in channel gating. *J Neurosci*. 2007;27:11641-11650.
32. Rohács T, Lopes CMB, Michailidis I, Logothetis DE. PI(4,5)P2 regulates the activation and desensitization of TRPM8 channels through the TRP domain. *Nat Neurosci*. 2005;8:626-634.
33. Paulsen CE, Armache J-P, Gao Y, Cheng Y, Julius D. Structure of the TRPA1 ion channel suggests regulatory mechanisms. *Nature*. 2015;520:511-517.
34. Liao M, Cao E, Julius D, Cheng Y. Structure of the TRPV1 ion channel determined by electron cryo-microscopy. *Nature*. 2013;504:107-112.
35. Gao Y, Cao E, Julius D, Cheng Y. TRPV1 structures in nanodiscs reveal mechanisms of ligand and lipid action. *Nature*. 2016;534:347-351.

SUPPORTING INFORMATION

Additional supporting information may be found online in the Supporting Information section.

How to cite this article: Xian W, Wang H, Moretti A, Laugwitz K-L, Flockerzi V, Lipp P. Domain zipping and unzipping modulates TRPM4's properties in human cardiac conduction disease. *The FASEB Journal*. 2020;34:12114–12126. https://doi.org/10.1096/fj.202000097RR